IEEE Access
Multidisciplinary | Rapid Review | Open Access Journal

SPECIAL SECTION ON ADVANCED ENERGY CONVERSION SYSTEMS BASED ON MULTI-PORT ELECTRICAL MACHINES

Received June 2, 2021, accepted June 14, 2021, date of publication June 22, 2021, date of current version July 5, 2021.

Digital Object Identifier 10.1109/ACCESS.2021.3091466

An Asymmetric-Primary Axis-Flux Hybrid-Excitation Generator for the Vertical Axis Wind Turbine

JING LIU[1], (Member, IEEE), QIANG ZHANG[2], RUNBO WANG[1], JILONG HU[1], LIJUN ZHANG[1], AND BAOPING CAI[1], (Member, IEEE)

[1]College of Mechanical and Electrical Engineering, China University of Petroleum, Qingdao 257061, China
[2]College of New Energy, China University of Petroleum, Qingdao 257061, China

Corresponding author: Jing Liu (ljdq98@163.com)

This work was supported in part by the National Natural Science Fund of China under Grant 51707204, in part by the Fundamental Research Funds for the Central Universities under Grant 18CX02092A, and in part by the National Key Research and Development Program of China under Grant 2019YFE0105100.

ABSTRACT Axis-flux wind generators are widely used in vertical axis wind turbines given their high generator diameter-to-length and power-to-weight ratios, flexible field and winding design, improved cooling, and possibility of modular construction. In this paper, an asymmetric-primary axis-flux hybrid-excitation generator (APAFHG) is proposed to provide a controllable maglev force that compensates for the ripple of axial force fluctuation. First, the operation principle of the proposed generator is introduced. No-load performance influenced by direct current (DC) excitation is obtained by using the 3D finite element method (3D-FEM). Second, the load performances are analyzed under two typical operation statuses, namely, symmetrical pure resistance load and $i_d = 0$ control strategy load. An alternating current (AC) excitation method is then comparatively analyzed to increase the output power under the maximum armature current. Third, based on the dq axes dynamic mathematical model, the quantitative calculations of levitation force and torque characteristics are deprived and then tested and verified by using the finite element analysis results. These results show that the proposed generator can be implemented for the decoupling control operation of power and levitation forces and is suitable for vertical axis wind turbines.

INDEX TERMS Vertical axis wind turbine, axis-flux generator, hybrid-excitation, force performance, dynamic mathematical model.

I. INTRODUCTION

Wind turbines are mainly categorized into horizontal and vertical axis wind turbines [1]. Vertical axis wind turbines are known for their many advantages, including their independence with respect to wind direction, stable force, easy installation and maintenance, and low starting wind speed [2], [3]. These turbines are especially suitable for offshore floating wind power systems [4], [5]. Direct-drive turbines without a gearbox have been extensively studied for their high reliability, low maintenance cost, and high efficiency [6]. Compared with traditional radial flux rotation generators, axial flux generators have a higher generator diameter-to-length ratio and are suitable for direct coupled wind turbine applications, such as vertical axis and direct-coupled wind turbines [7]–[9].

The associate editor coordinating the review of this manuscript and approving it for publication was Wei Xu.

These generators also have a large power-to-weight ratio, highly flexible field and winding design, improved cooling, and potential application in modular construction.

Accordingly, different axial flux generators have been proposed for direct-drive wind power generation, such as axial flux permanent magnet generators, axial flux doubly fed induction generators, and axial flux flux-switching generators [9]–[13]. With their high power density, permanent magnet synchronous generators have received widespread attention and application in vertical axis wind turbines.

However, the direct coupling of the high-power axial flux permanent magnet synchronous generator and wind turbine may introduce problems in starting the wind turbine. To improve the starting performance of vertical axis wind turbines, maglev technology is considered to reduce the starting resistance torque [14]. However, traditional maglev devices with dynamic air gap adjustment have a complex structure

and coupling output power [15], [16]. To address this problem, an asymmetric-primary axis-flux hybrid-excitation generator (APAFHG) is proposed in this paper. This proposed generator can generate a levitation force with fixed air gap length and is designed to realize a decoupling control of levitation force and output power by using asymmetric primary and hybrid excitation.

This paper aims to develop a new axis-flux hybrid-excitation generator for wind turbine based on traditional permanent magnet synchronous generators. The asymmetric-primary design generates a controllable suspension levitation force to compensate for the ripple of axial force fluctuation. Upper and lower stators are employed to supply different output power under varying axial maglev forces. Two excitation current injection methods, namely, DC excitation current injection and AC excitation current injection, can be used. DC excitation can realize a real-time control of suspension force and decoupling with the electromagnetic torque, whereas AC excitation can increase the output power under the maximum armature current. However, implementing excitation winding in the proposed generator will change the force and torque performance. To analyze the force performance of the proposed generator, 3D FEM is implemented in this paper.

First, the topology and operation principle of the proposed APAFHG are introduced. Second, two excitation characteristics are comparatively analyzed and discussed by FEM. Third, based on the dynamic mathematical model of the proposed generator, in the *dq* axis frame obtained by rotor-flux vector orientation, the quantitative calculations of levitation force and torque are deprived. The dynamic levitation force of the proposed generator calculated by the deprived formula is then verified based on the simulation results obtained by FEM. Results show that the proposed generator can be implemented in the decoupling control operation of power and levitation force. The proposed APAFHG is suitable for vertical axis wind turbines.

II. OPERATION PRINCIPLE

A typical vertical axis wind turbine is composed of a wind turbine and a generator. Axis-flux generators are suitable for those vertical axis wind turbines with short axial length and easily module a combination of multiple generators according different power requirements. Fig. 1 shows the structure of the proposed APAFHG with a vertical axis wind turbine.

The proposed generator has an upper and lower stator and one rotor, which in turn comprises permanent magnets, rotor teeth, and yoke back iron. The rotor teeth are made of a steel sheet, whereas the yoke is made of a whole piece of steel. To measure the levitation force acting on the rotor, two stators with different diameters are used. However, to keep the terminal voltage of two stators consistent, the winding turns of upper and lower stators should be different. The cross-section of the proposed generator is shown in Fig. 2. Stator teeth are made of steel sheets, whereas the stator yoke is made of a whole piece of steel. The armature windings

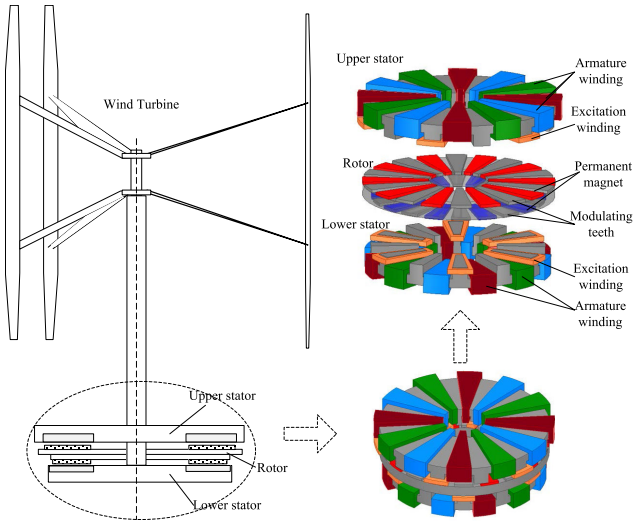

FIGURE 1. Structure of the proposed APAFHG.

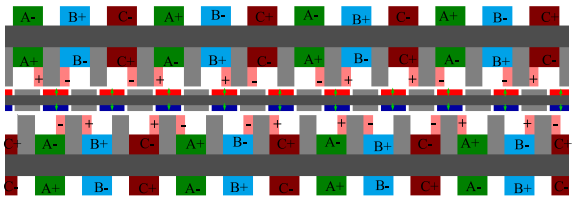

FIGURE 2. Circumferential cross section of the proposed generator.

are wound around on the stator yoke slots, and the excitation windings are wound around the stator teeth. Compared with the rotor excitation generator, this design facilitates thermal management due to the easy heat dissipation in its stator [17]. Instead of both winding armature and excitation on the stator teeth, an improved insulation between the armature and excitation windings can be achieved for a limited contact area. Two stators have a half slot pitch shift to reduce the cogging torque. The current direction of excitation and the magnetization direction of the permanent magnet are shown in Fig. 2.

The relationship among the stator tooth number, rotor pole pair, and stator pole pair is given as

$$p_r = |p_n \pm p_s| \tag{1}$$

where p_{r} and p_{s} are the pole pair numbers of the rotor and stator armature, whereas the tooth number of the stator is p_{n}.

This design creates a magnetic field modulation effect, which can increase the magnetic field change rate under low direct drive speed and increase the output voltage.

The basic parameters of the proposed APAFHG are listed in Table.1. The magnetic-field distributions under 2D and 3D models obtained by commercial FEM software are shown in Fig. 3, whereas the distribution of magnetic lines under different excitation currents is shown in Fig. 4.

Fig. 3 and Fig. 4 show that the upper and lower stators have an independent parallel magnetic circuit injecting different

TABLE 1. Basic dimension parameters of the proposed generator.

Parameter	Unit	Value
External diameter of upper stator	mm	200
Internal diameter of upper stator	mm	100
External diameter of lower stator	mm	180
Internal diameter of lower stator	mm	100
Yoke thickness of upper stator	mm	25
Yoke thickness of lower stator	mm	25
Number of upper stator slots		12
Number of lower stator slots		12
Depth of upper stator slot	mm	40
Depth of lower stator slot	mm	40
Tooth width / slot width ratio		9/16
Number of pole pairs		10
Polar arc coefficient		0.8
Thickness of permanent magnet	mm	6
Excitation turns per teeth		150
Armature turns per phase of upper stator		400
Armature turns per phase of lower stator		540

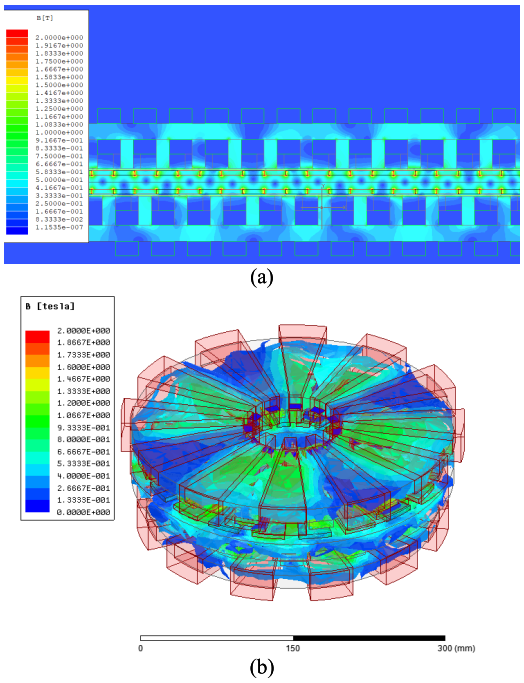

FIGURE 3. Magnetic-field distributions under 2D and 3D models. (a) 2D magnetic-field distributions; and (b) 3D magnetic-field distributions.

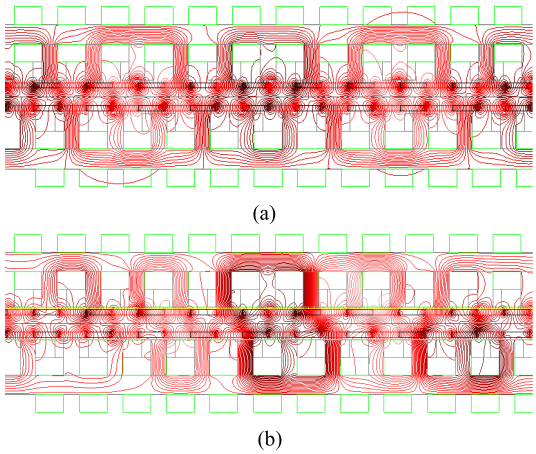

FIGURE 4. Distribution of magnetic lines under different excitation currents. (a) without DC excitation; and (b) with DC excitation.

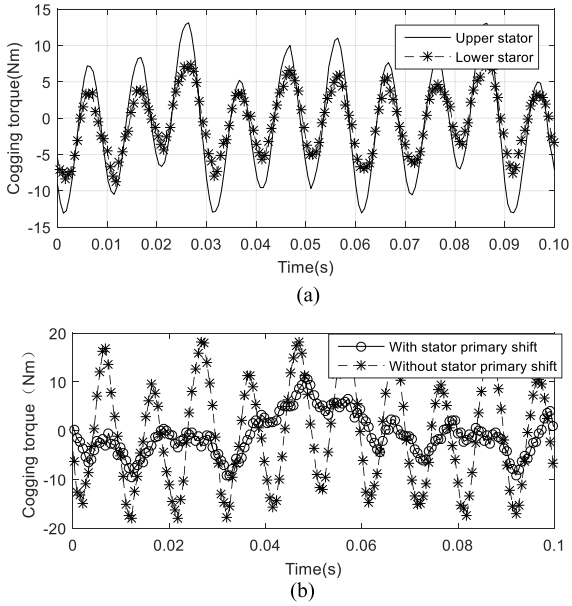

FIGURE 5. Cogging torque of the proposed generator. (a) Cogging force between two stators and rotor without a half slot pitch shift; and (b) total cogging force with and without a half slot pitch shift.

DC excitation currents, which facilitates the decoupling of the output power of both upper and lower stators. Instead of around the tooth, the winding wound is around the yokes given that the magnetic field intensity of yokes in one phase winding is complementary, such as that of yokes in phase A. The flux linkage in one phase is not changed with DC excitation current and contains a small harmonic component. However, the electromotive force of tooth winding is generally rich in low-order harmonics, which will cause torque ripple and harm the generator.

The cogging torque is caused by the slot effect among the upper stator, lower stator, and rotor. The cogging force between one stator and mover is affected by the polar arc coefficient and pole slot ratio. However, adjusting the polar arc coefficient and pole slot ratio inevitably reduces the voltage and flux in the armature. By using the half slot pitch shift, the cogging force between two states and the rotor can compensate each other, and the voltage amplitude of the two stators remains unchanged. The cogging force between two stators and the rotor and the total cogging force with and without a half slot pitch shift are obtained by using transition 3D FEM as shown in Fig. 5.

As shown above, the cogging torque can be reduced with a half slot pitch shift.

The upper and lower stators are two independent generators with only levitation force generating a superposition effect. Therefore, a single-side stator generator is used to

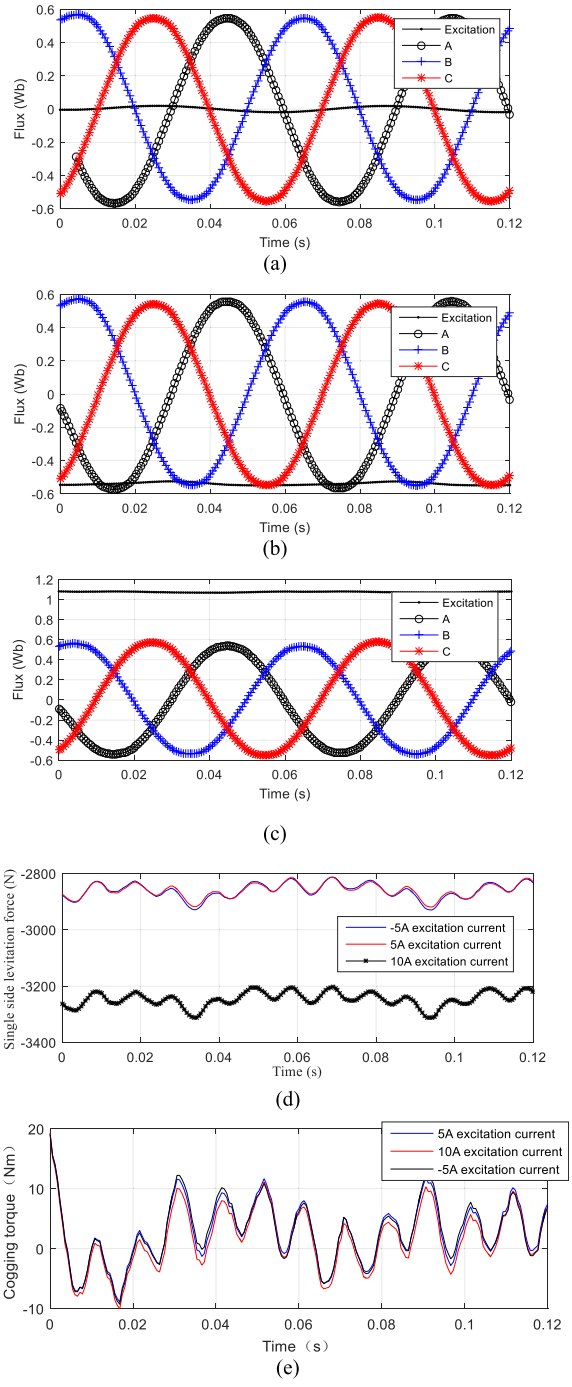

FIGURE 6. No-load performance of the proposed generator. (a) Flux linkage without DC excitation; (b) flux linkage with -5A DC excitation; (c) flux linkage with 10A DC excitation; (d) fingle-side levitation force; and (e) single-side cogging torque under different DC excitations.

study the proposed generator and to simplify the 3D simulation model.

Under a constant rotational speed condition, the no-load performance, which includes flux linkage, levitation force, and cogging torque under different DC excitation currents, is recorded by using transition 3D FEM as shown in Fig. 6.

Fig. 6(a) shows the flux linkage in the armature and excitation windings. The flux linkage in the excitation windings is almost zero, which is caused by permanent magnets, thereby we suggest the absence of any interaction between permanent magnet flux linkage and excitation winding. Meanwhile, Fig. 6(b) and 6(c) show the flux linkage in the armature and excitation windings under different DC excitation currents. Fig. 6(a) to 6(c) shows that the flux linkages in the armature are consistent and only decided by the permanent magnet flux linkage and does not change along with the DC excitation current. Therefore, DC excitation current has no effect on armature flux linkage.

Fig. 6(e) and 6(d) show the single-side levitation force and cogging torque with DC excitation current. The levitation force changes along with the DC excitation current, whereas the cogging force does not change because the air gap magnetic density increases along with the DC excitation current and the composite vector of the cogging force caused by the DC excitation current is zero.

Therefore, the load torque is independent of the DC excitation current given that the flux linkage in the armature and cogging force is not affected by the DC excitation current. However, the levitation force changes along with the DC excitation current. In sum, the output power is decided by both torque and rotation speed, whereas levitation fore is decided by DC excitation.

III. EXCITATION CHARACTERISTICS

A. DC EXCITATION CHARACTERISTICS

Two typical operation statuses of the generator are used in conventional wind power generation systems, namely, off- and on-grid as shown in Fig. 7. One is a pure resistance load operation where three phases of symmetrical pure resistance load are implemented, whereas the other is a maximum wind energy capturing operation. The rotor-flux vector orientation is always used in generator-side converter controller. The *dq* axis current is always controlled to capture maximum wind energy in the rotor rotating along the *dq* axis frame.

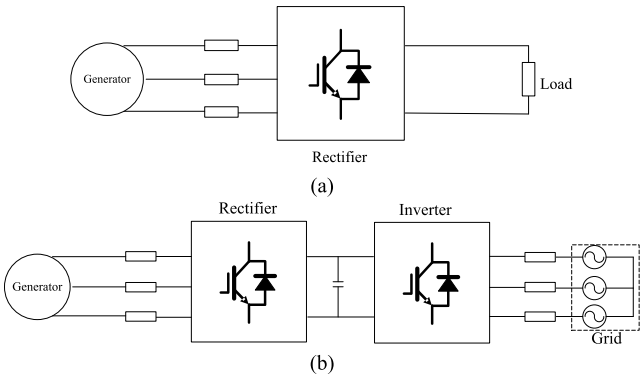

FIGURE 7. Two typical operation statuses. (a) Resistance load condition with off grid; and (b) maximum wind energy operation on grid.

Under the constant pure resistance load condition, the levitation force and flux linkage of the proposed generator with DC excitation current are obtained by FEM and shown in Fig. 8.

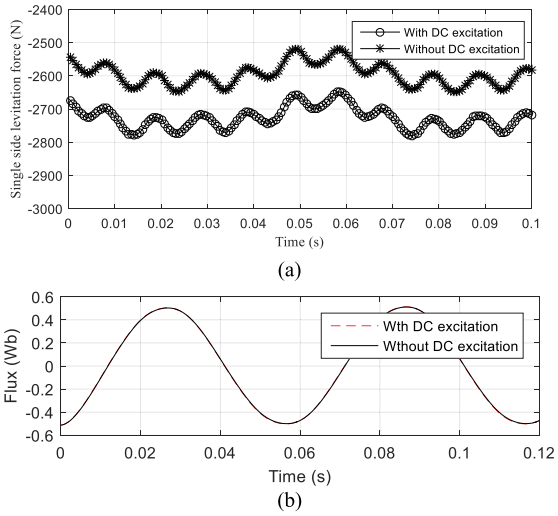

FIGURE 8. Load performance under pure resistance load. (a) Levitation force; and (b) flux linkage.

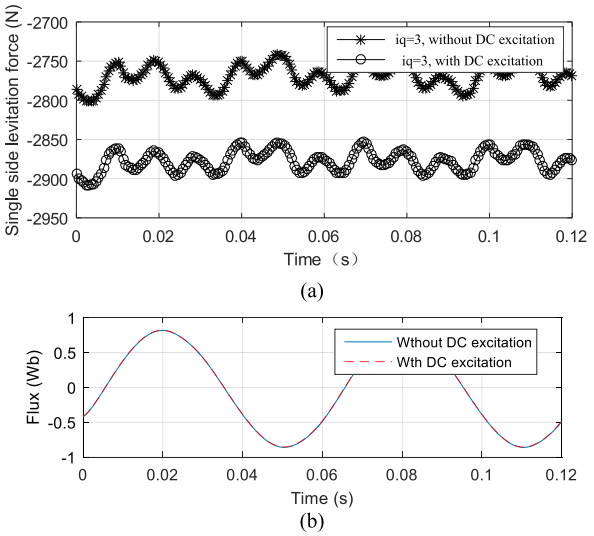

FIGURE 9. Load performance under the $i_d = 0$ control strategy. (a) Levitation force; and (b) flux linkage.

When the resistance load is constant, the flux linkage of the armature is constant with or without the DC excitation current. The levitation force changes along with the DC excitation current when the magnetic field of the stator core is not saturated. Therefore, under the pure resistance load condition, the output power is decided by the resistance load. However, the levitation force can be controlled by the DC excitation current, which is completely decoupled from the output power.

Under the pure resistance load condition, achieving maximum energy capture becomes difficult. Therefore, the dq axes current is controlled to capture maximum wind energy by using a controlled rectifier in the machine-side control system. A typical control is the $i_d = 0$ control strategy, which reference value of d axis current is set to zero, whereas the q axis current is controlled to change along with wind energy according to the wind energy utilization factor. Under the $i_d = 0$ control strategy, the levitation force and flux linkage of the proposed generator are shown in Fig. 9.

Flux linkage is decided by the armature current and PM, which is similar to the traditional generator. Under constant q-axis current, the DC excitation current only changes the levitation force. However, the levitation force changes also along with the q-axis current. Therefore, the output power can be controlled by the armature current similar to traditional generators. Based on the levitation force generated by the q-axis current that corresponds to controlled power, levitation force decoupling control can be realized by the DC excitation current. Therefore, maximum wind energy capture and levitation force can be decoupled through both armature and DC excitation currents.

B. AC EXCITATION CHARACTERISTICS

DC excitation can be implemented to control the levitation force. The output power is decoupled with levitation force by using DC excitation. However, the output power does not increase if the armature current reaches the upper limit. To increase the output power under the maximum armature current, an AC excitation method is proposed. AC excitation currents are initially injected into excitation windings to increase the flux linkage in armature windings. The phase angle of the AC excitation currents is related to the mover position. The flux linkage in the excitation winding caused by AC excitation current is implemented to realize the magnetization or demagnetization of the armature flux linkage, which is in the same or opposite direction as the PM flux linkage. Therefore, the output power range can be increased. The AC excitation windings are shown in Fig. 10.

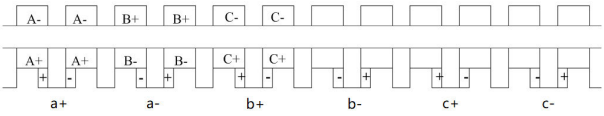

FIGURE 10. AC excitation winding.

Fig. 11 shows the flux linkage, voltage, and levitation force of the proposed generator as obtained by FEM.

As we can see from the performance under AC excitation, the flux linkage and voltage can be effectively changed, and then the output power of the generator subsequently increases. However, the levitation force changes along with the AC excitation current. A coupling is observed between levitation force and output power. Therefore, decoupling may be used to control the levitation force and output power.

IV. FORCE AND TORQUE CHARACTERISTIC ANALYSIS

The levitation force and torque characteristics can be quantitatively obtained by using a dynamic mathematical model under the dq axis frame. Therefore, the levitation force and torque under DC and AC excitations are derived based on dynamic mathematical formulas under the rotor field orientation dq axis frame.

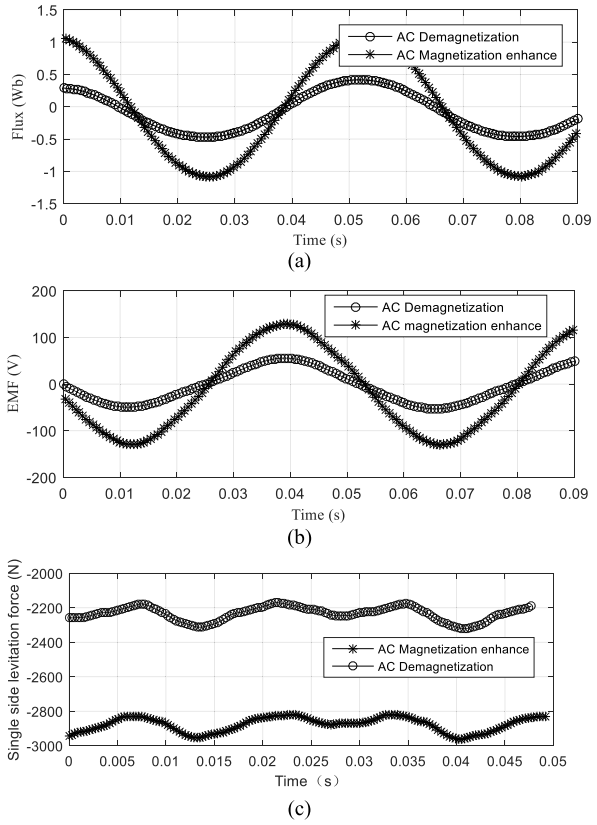

FIGURE 11. Performance under AC excitation. (a) Flux linkage; (b) phase voltage; and (c) levitation force.

Under the $i_d = 0$ control strategy, the on-load performance of the torque and levitation force of the proposed generator is derived.

The voltage equation under the dq axis frame is

$$\begin{aligned} u_d &= \frac{d\psi_d}{dt} - \psi_q \frac{d\theta}{dt} + Ri_d \\ u_q &= \frac{d\psi_q}{dt} + \psi_d \frac{d\theta}{dt} + Ri_q \end{aligned} \tag{2}$$

where ψ_d, ψ_q represent the d and q axis flux, θ represent the rotor position angle, R represents the d or q axis armature resistance, and i_d, i_q represent the d and q axis current.

The d and q axis flux linkage are expressed respectively as

$$\begin{aligned} \psi_d &= L_d i_d + \psi_{\text{pm}} \\ \psi_q &= L_q i_q \end{aligned} \tag{3}$$

where L_d, L_q represent the d and q axis inductance, whereas ψ_{pm} represents the permanent magnet flux linkage that can be defined as $\psi_{\text{pm}} = L_f i_f$. L_f represents the equivalent excitation inductance of PM.

Therefore, the torque can be calculated as

$$T_{\text{e}} = \frac{p_e}{\omega} = \frac{p_{e1} + p_{e2}}{\omega} \tag{4}$$

where p_{e1} and p_{e2} represent the instantaneous powers in the armature winding caused respectively by PM and excitation winding, and ω represent the angular velocity.

According to the virtual work method, the active power in normal direction caused by normal force can be expressed as three parts by

$$P_{\text{y}} = P_{\text{y1}} + P_{\text{y2}} + P_{\text{y3}} \tag{5}$$

where $P_{\text{y1}}, P_{\text{y2}}, P_{\text{y3}}$ represent the virtual active powers caused by armature winding, excitation winding, and PMs. And there are

$$\begin{aligned} P_{\text{y1}} &= \left(i_{d1} \frac{d\psi_{d1}}{dh} + i_{q1} \frac{d\psi_{q1}}{dh} \right) \frac{\partial h}{\partial t} \\ P_{\text{y3}} &= \left(i_f \frac{\partial \psi_f'}{\partial h} \right) \frac{\partial h}{\partial t} \end{aligned} \tag{6}$$

where h represents the air gap length, i_{d1} and i_{q1} are d-axis and q-axis component of the armature current, ψ_{d1} and ψ_{q1} are d-axis and q-axis component of armature flux linkage.

When we inject DC excitation current into the armature windings, P_{y2} can be written by

$$P_{\text{y2dc}} = \left(i_{dc} \frac{\partial \psi_{dc}}{\partial h} \right) \frac{\partial h}{\partial t} \tag{7}$$

where i_{dc} represents the DC excitation current, ψ_{dc} represents the excitation winding flux linkage.

When we inject AC excitation current into the armature windings, P_{y2} can be written by

$$P_{\text{y2ac}} = \left(i_{d2} \frac{d\psi_{d2}}{dh} + i_{q2} \frac{d\psi_{q2}}{dh} \right) \frac{\partial h}{\partial t} \tag{8}$$

where i_{d2} and i_{q2} represent the d-axis and q-axis component of AC exciting current, ψ_{d2} and ψ_{q2} represent the d-axis and q-axis component of excitation winding flux linkage.

Thus, the normal forces caused by armature current, excitation winding, and PMs, can be expressed respectively as

$$\begin{aligned} F_{n1} &= i_{d1} \frac{d\psi_{d1}}{dh} + i_{q1} \frac{d\psi_{q1}}{dh} \\ &= \left(i_{d1}^2 + i_f i_{d1} \right) \frac{\partial L_{d1}}{\partial h} + i_{q1}^2 \frac{\partial L_{q1}}{\partial h} \end{aligned} \tag{9}$$

$$\begin{aligned} F_{n2ac} &= i_{d2} \frac{d\psi_{d2}}{dh} + i_{q2} \frac{d\psi_{q2}}{dh} \\ F_{n2dc} &= i_{dc} \frac{\partial \psi_{dc}}{\partial h} \end{aligned} \tag{10}$$

$$\begin{aligned} F_{n3} &= i_f \frac{\partial \psi_f'}{\partial h} = i_f \frac{\partial \left(\psi_f + \psi_{df} \right)}{\partial h} \\ &= i_f \frac{\partial \left(L_f i_f + i_{d1} M_{af} \right)}{\partial h} \\ &= \left(i_f^2 + i_f i_{d1} \right) \frac{\partial L_{d1}}{\partial h} \end{aligned} \tag{11}$$

where L_{d1}, L_{q1} represent the d-axis and q-axis inductance of armature, M_{af} represent the equivalent mutual inductance between armature and PM, and there is $M_{af} = L_{d1}$.

When the excitation windings are injected into DC current, armature flux does not interlink with the excitation winding, thus p_{e2} is zero. Therefore, the torque is

$$T_{\text{edc}} = \frac{p_{e1}}{\omega} = \frac{3p_{\text{n}}}{2} \left(\psi_{\text{pm}} i_{q1} + \left(L_{d1} - L_{q1} \right) i_{d1} i_{q1} \right) \tag{12}$$

where p_n represents the number of pole pair. And the normal force caused by armature and PMs is

$$F_{n13} = \left(i_{d1}^2 + i_f^2 + 2i_f i_{d1}\right)\frac{\partial L_{d1}}{\partial h} + i_{q1}^2\frac{\partial L_{q1}}{\partial h} \tag{13}$$

Normal force caused by the excitation current i_{dc} is

$$F_{n2dc} = i_{dc}\frac{\partial \psi_{dc}}{\partial h} = i_{dc}\frac{\partial L_{dc} i_{dc}}{\partial h} = i_{dc}^2\frac{\partial L_{dc}}{\partial h} \tag{14}$$

where L_{dc} represents the self-inductance of the excitation windings. The total normal force can be calculated by

$$F_n' = \left(i_{d1} + i_f\right)^2\frac{\partial L_{d1}}{\partial h} + i_{q1}^2\frac{\partial L_{q1}}{\partial h} + i_{dc}^2\frac{\partial L_{dc}}{\partial h} \tag{15}$$

When the excitation windings are injected into AC current, the magnetic field caused by AC excitation rotates synchronously with PM magnetic field, which leads to a zero i_{q2}, but p_{e2} is not zero because the armature flux interlinks with the excitation winding. Therefore, we can obtain the torque under AC excitation by

$$\begin{aligned} T_{\text{eac}} &= \frac{p_{e1} + p_{e2}}{\omega} \\ &= \frac{3p_n}{2}\left((\psi_{\text{pm}} + i_{d2}L_{d2})i_{q1} + (L_{d1} - L_{q1})i_{d1}i_{q1}\right) \end{aligned} \tag{16}$$

The total normal force can be calculated as

$$F_n'' = \left(i_{d1} + i_f + i_{d2}\right)^2\frac{\partial L_{d1}}{\partial h} + i_{q1}^2\frac{\partial L_{q1}}{\partial h} \tag{17}$$

To verify the levitation force formula, the levitation force under different i_d and i_q currents are obtained by using 3D transient FEM. The levitation forces under different i_d currents are shown in Fig. 12(a) when $i_q = 0$. Fig. 12(b) shows the levitation forces under different i_q currents when $i_d = 0$. Fig. 12(c) shows the average levitation force calculated by (15) and FEM to contrast.

First, the results obtained by the derived formula are consistent with the simulation results obtained under a low armature current. However, a small difference can be observed between the calculated values and simulation results, which can be ascribed to the increasing flux leakage caused by the local saturation of the stator teeth.

In addition, the levitation force caused by the d-axis current is much greater than that caused by the q-axis current, and is proportional to the d-axis current. It is because of the smaller changing rate of the q-axis inductance with the air gap.

Fig. 13 shows the torques under different q-axis currents with constant speed. The torque are proportional to the d-axis current. The output power is decided by the q-axis current. Therefore, under the $i_d = 0$ control strategy, the output power can be controlled by the q-axis current, whereas the levitation force can be controlled by the DC current. The levitation force generated by the q-axis current can be regarded as a disturbance. If the d-axis current is changed, then the levitation force reference should be calculated in real time, and a DC current reference should be given to control the levitation force.

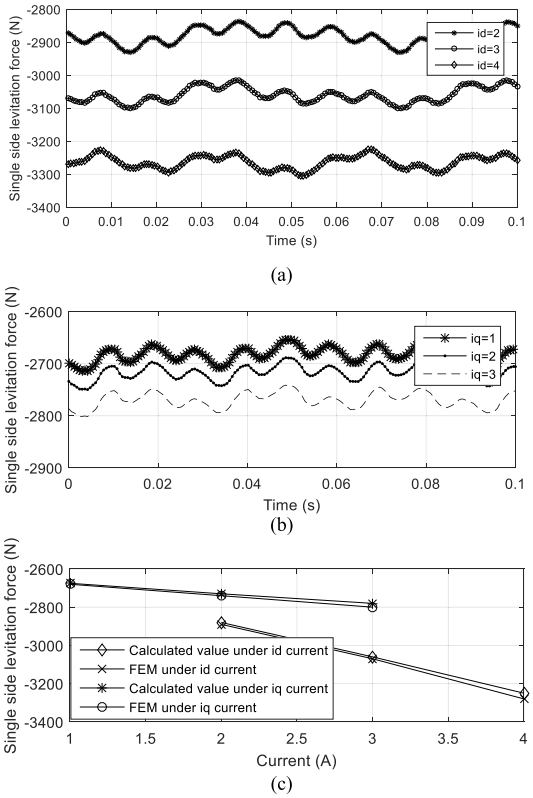

FIGURE 12. Dynamic levitation force. (a) Levitation forces under different id currents; (b) levitation forces under different i_q currents; and (c) levitation force calculation comparison.

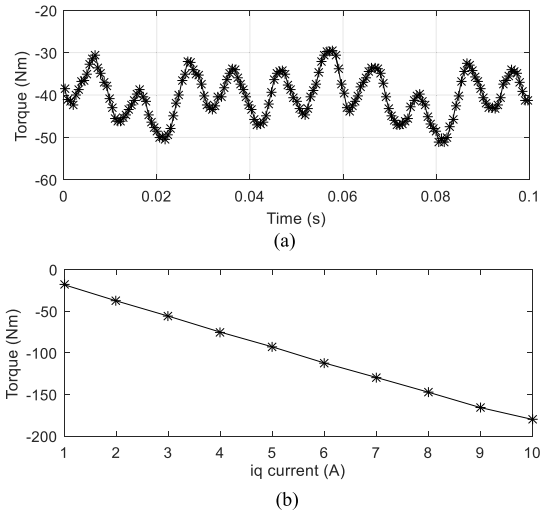

FIGURE 13. Torque under different loads. (a) Torque under $i_q = 4$A; and (b) torque under i_q current.

V. CONCLUSION

This paper proposed APAFHG and analyzed its 3D electromagnetic field and no-load performances. By using a half slot pitch shift, the cogging torque is reduced effectively. Both the flux linkage and cogging torque remain unchanged along with changing DC excitation current. Under two typical operation statuses, the on-load performance with the DC and AC excitation injecting method is comparatively studied.

DC excitation can be implemented to decouple-control the levitation force, whereas AC excitation can be implemented to change the output power under the same armature current and subsequently expand the power range. Quantitative calculations of the levitation force and torque are obtained by using the dynamic mathematical model under the dq axis frame. Levitation force and torque are analyzed under different i_d and i_q currents to verify the accuracy of the derived formula. Results show that the proposed generator is suitable for vertical axis wind turbines with its easily decoupling of the power and levitation force

REFERENCES

[1] S. Eriksson, H. Bernhoff, and M. Leijon, "Evaluation of different turbine concepts for wind power," *Renew. Sustain. Energy Rev.*, vol. 12, no. 5, pp. 1419–1434, Jun. 2008.

[2] M. R. Islam, S. Mekhilef, and R. Saidur, "Progress and recent trends of wind energy technology," *Renew. Sustain. Energy Rev.*, vol. 21, pp. 456–468, May 2013.

[3] B. Hand, A. Cashman, and G. Kelly, "A low-order model for offshore floating vertical axis wind turbine aerodynamics," *IEEE Trans. Ind. Appl.*, vol. 53, no. 1, pp. 512–520, Jan. 2017.

[4] U. S. Paulsen, H. A. Madsen, K. A. Kragh, P. H. Nielsen, I. Baran, J. Hattel, E. Ritchie, K. Leban, H. Svendsen, and P. A. Berthelsen, "Deep Wind-from idea to 5 MW concept," *Energy Procedia*, vol. 53, pp. 23–33. 2014.

[5] M. Borg, A. Shires, and M. Collu, "Offshore floating vertical axis wind turbines, dynamics modelling state of the art. Part I: Aerodynamics," *Renew. Sustain. Energy Rev.*, vol. 39, pp. 1214–1225, Nov. 2014.

[6] J. W. Chen, J. Chen, and C. Y. Gong, "On optimizing the aerodynamic load acting on the turbine shaft of PMSG-based direct-drive wind energy conversion system," *IEEE Trans. Ind. Electron.*, vol. 61, no. 8, pp. 4022–4033, Aug. 2009.

[7] T. F. Chan and L. L. Lai, "An axial-flux permanent-magnet synchronous generator for a direct-coupled wind-turbine system," *IEEE Trans. Energy Convers.*, vol. 22, no. 1, pp. 86–94, Mar. 2007.

[8] S. Brisset, D. Vizireanu, and P. Brochet, "Design and optimization of a nine-phase axial-flux PM synchronous generator with concentrated winding for direct-drive wind turbine," *IEEE Trans. Ind. Appl.*, vol. 44, no. 3, pp. 707–715, May-Jun. 2008.

[9] M. Y. Lin, L. Hao, X. Li, X. M. Zhao, and Z. Q. Zhu, "A novel axial field flux-switching permanent magnet wind power generator," *IEEE Trans. Magn.*, vol. 47, no. 10, pp. 4457–4460, Sep. 2011.

[10] V. Naeini and M. Ardebili, "New axial flux PM less synchronous machine with concentrated DC field on stator," *Int. J. Electr. Power Energy Syst.*, vol. 67, pp. 651–658, May 2015.

[11] M. J. Khan, M. T. Iqbal, and J. E. Quaicoe, "Dynamics of a vertical axis hydrokinetic energy conversion system with a rectifier coupled multi-pole permanent magnet generator," *IET Renew. Power Gener.*, vol. 4, no. 2, pp. 116–127, 2010.

[12] P. Xu, K. Shi, F. Bu, D. Zhao, Z. Fang, R. Liu, and Y. Zhu, "A vertical-axis off-grid squirrel-cage induction generator wind power system," *Energies*, vol. 9, no. 10, p. 822, Oct. 2016.

[13] R. Wang, L. Brönn, S. Gerber, and P. Tlali, "An axial flux magnetically geared permanent magnet wind generator," *IEEJ Trans. Electr. Electron. Eng.*, vol. 10, no. S1, pp. S123–S132, Oct. 2015.

[14] G. Ahmad and U. Amin, "Design, construction and study of small scale vertical axis wind turbine based on a magnetically levitated axial flux permanent magnet generator," *Renew. Energy*, vol. 101, pp. 286–292, Feb. 2017.

[15] G. Shrestha, H. Polinder, D.-J. Bang, and J. A. Ferreira, "Structural flexibility: A solution for weight reduction of large direct-drive wind-turbine generators," *IEEE Trans. Energy Convers.*, vol. 25, no. 3, pp. 732–740, Sep. 2010.

[16] C. V. Aravind, R. Rajparthiban, R. Rajprasad, and Y. V. Wong, "A novel magnetic levitation assisted vertical axis wind turbine—Design procedure and analysis," in *Proc. IEEE 8th Int. Colloq. Signal Process. Appl.*, Mar. 2012, pp. 93–98.

[17] Z. Q. Zhu, H. Hua, D. Wu, J. T. Shi, and Z. Z. Wu, "Comparative study of partitioned stator machines with different PM excitation stators," *IEEE Trans. Magn.*, vol. 52, no. 1, pp. 2070–2199, Sep. 2016.

JING LIU (Member, IEEE) was born in Baoding, Hebei, China, in 1980. She received the Ph.D. degree from the College of Energy and Electrical Engineering, Hohai University. She has been a Teacher with the College of Mechanical and Electrical Engineering, China University of Petroleum, since 2002. Her research interests include the design of special motor, optimization and calculation of the electromagnetic field in motor, design and control of magnetic suspension systems, and wind generator.

QIANG ZHANG received the B.S. degree in electrical engineering and automation from the China University of Petroleum, Qingdao, China, in 2019, where he is currently pursuing the master's degree in electrical engineering. His current research interests include analysis and control of magnetic levitation machines and wind power generation.

RUNBO WANG is currently pursuing the bachelor's degree in mechanical design, manufacturing, and automation from the China University of Petroleum. He has won many scholarships and participated in many science and technology competitions. His research interests include mechanical design and automatic control of electromechanical systems.

JILONG HU is currently pursuing the bachelor's degree in mechanical design, manufacturing and automation from the China University of Petroleum. He has won many scholarships and participated in many science and technology competitions. His research interests include mechanical design and automatic control of wind generator systems.

LIJUN ZHANG was born in Pingyin, Shandong, China, in 1977. He received the Ph.D. degree from the School of Mechanical Engineering, Xian Jiaotong University. He has been a Professor with the College of Mechanical and Electrical Engineering, China University of Petroleum, since 2015. His research interests include renewable energy power generation technology and equipment and intelligent manufacturing.

BAOPING CAI (Member, IEEE) received B.S. degree in mechanical design, manufacturing, and automation and the Ph.D. degree in mechanical and electronic engineering from the China University of Petroleum, in 2006 and 2012, respectively. From 2013 to 2014, he was a Lecturer with the China University of Petroleum, where he is currently a Professor. His research interests include reliability engineering, fault diagnosis, risk analysis, and Bayesian networks methodology and application.